

Contents lists available at [ScienceDirect](https://www.sciencedirect.com)

# Theoretical and Applied Fracture Mechanics

journal homepage: [www.elsevier.com/locate/tafmec](http://www.elsevier.com/locate/tafmec)

## Structural integrity assessment of additively manufactured ABS, PLA and graphene reinforced PLA notched specimens combining Failure Assessment Diagrams and the Theory of Critical Distances

S. Cicero<sup>\*</sup>, M. Sánchez, V. Martínez-Mata, S. Arrieta, B. Arroyo

LADICIM (Laboratory of Materials Science and Engineering), University of Cantabria, E.T.S. de Ingenieros de Caminos, Canales y Puertos, Av/ Los Castros 44, Santander, 39005 Cantabria, Spain

### ARTICLE INFO

#### Keywords:

Failure Assessment Diagram  
Graphene  
Additive manufacturing  
Fused deposition modelling  
Notch  
Theory of Critical Distances

### ABSTRACT

Failure Assessment Diagrams (FADs) are a widely used engineering tool for the analysis of structural components containing cracks, and are included in recognised structural integrity assessment procedures such as BS7910 and API 579 1/ASME FFS 1. Their consistency and reliability has been demonstrated over the years through numerous laboratory validation tests and industrial applications. Nevertheless, both their theoretical definition and their subsequent validation have been performed in metallic materials and, therefore, their use in other types of materials still requires theoretical support and experimental validation. Moreover, FADs have been initially defined for the analysis of crack-like defects, whereas there are many situations where the defects that are, or might be, responsible for structural failure are not necessarily cracks. This is the case of (non-sharp) defects with a finite radius on their tip, which here will be referred to as notches.

Simultaneously, additive manufacturing (AM) is an emergent technology that allows practically any type of geometry to be fabricated through a relatively simple process. One of the main AM techniques is fused deposition modelling (FDM), which consists in the extrusion of heated feedstock plastic filaments through a nozzle tip. The resultant printed materials have rather particular properties that are very dependent on the printing parameters and on the final state of internal defects. Concerning AM polymers and polymer-matrix composites, their use as structural materials, beyond their main current use in prototyping, requires the development of specific structural integrity assessment procedures.

This paper provides FAD analyses for three additively manufactured (FDM) materials containing U-shaped notches: ABS, PLA and graphene reinforced PLA. The results show that the FAD methodology may be applied for the estimation of fracture loads in these particular materials, as long as linear-elastic fracture toughness values are used.

### 1. Introduction

Structural failures are frequently associated with the presence of crack-like defects. With the aim of avoiding or predicting this kind of failures, assessment criteria are provided by structural integrity assessment procedures (e.g., FINDET FFS [1–2], BS7910 [3], R6 [4], API 579-1/ASME FFS-1 [5]), which are capable of determining whether the presence of a given crack in a specific component represents (or not) a structurally safe situation. In this sense, Failure Assessment Diagrams (FADs) are the most commonly used analysis tool.

However, there are numerous situations where the defects that jeopardise the structural integrity of a given component are not sharp (i.

e., crack-like defects). Some examples are mechanical damage, corrosion defects, fabrication defects or structural details (e.g., holes, corners, weld toes, etc.). If such defects are blunt, it may be excessively conservative to proceed on the assumption that they behave like sharp cracks and to apply fracture mechanics criteria (i.e., such an assumption may lead to unnecessary repairs or replacements, or to oversizing). As shown in the literature (e.g. [6–10]), components with non-sharp defects (here referred to as notches) exhibit an apparent fracture toughness that is greater than that obtained in cracked components. This generally has direct consequences on the load-bearing capacity of the component and also on the corresponding structural integrity assessments (e.g. [8]). The analysis of the fracture behavior of notched materials can be performed using different criteria. Some examples are the Theory of Critical

<sup>\*</sup> Corresponding author.

E-mail address: [ciceros@unican.es](mailto:ciceros@unican.es) (S. Cicero).

<https://doi.org/10.1016/j.tafmec.2022.103535>

Received 17 March 2022; Received in revised form 27 July 2022; Accepted 9 August 2022

Available online 12 August 2022

0167-8442/© 2022 The Author(s). Published by Elsevier Ltd. This is an open access article under the CC BY-NC-ND license (<http://creativecommons.org/licenses/by-nc-nd/4.0/>).

Nomenclature			
B	Specimen thickness	$P_Q$	load provided by the intersection of the load line and the line with a compliance 5 % greater than that of line elastic part of the load line
E	Young's modulus	J	applied J-integral
$K_{mat}$	material fracture toughness in stress intensity factor units	$J_e$	elastic component of J
$K_{mat}^N$	material fracture resistance in notched conditions (in stress intensity factor units)	$J_{mat}$	material fracture toughness in J units
$K_r$	fracture ratio of applied KI to fracture toughness	L	critical distance
$K_I$	applied stress intensity factor	$\rho$	notch radius
$L_r$	ratio of applied load to limit load (or reference stress to yield stress)	$\sigma_u$	ultimate tensile strength
$L_{r,max}$	maximum value of $L_r$ in a FAD	$\sigma_y$	yield stress
P	applied load	$\sigma_0$	inherent strength
$P_{est}$	estimation of the load bearing capacity	AM	Additive Manufacturing
$P_{exp}$	experimental load bearing capacity	FAD	Failure Assessment Diagram
$P_L$	limit load	FAL	Failure Assessment Line
		FDM	Fused Deposition Modeling
		SENB	Single Edge Notched Bending (specimen)

Distances (TCD) (e.g., [6,8]), Process Zone models (e.g., [11,12]), statistical models (e.g., [13,14]), or the Strain Energy Density (SED) criterion (e.g., [15,16]), among others. The Theory of Critical Distances (TCD) is extensively explained and validated in [6], demonstrating its great potential to solve engineering problems and to provide scientific insights. In any case, these different fracture criteria may be used to generate structural integrity assessment criteria addressing the specific nature of notch-type defects, as proposed in [8] through the combination of FADs and the TCD.

Moreover, the above-mentioned structural integrity assessment procedures address, exclusively, the evaluation of metallic materials, principally steels and aluminium alloys. However, the use of non-metallic materials in structural applications is increasing in recent years, making it essential to develop structural integrity assessment tools for these sorts of materials. Some research has been published providing FAD assessments of non-metallic materials containing crack-like defects, generally [8,17,18] using the same FADs provided by the main structural integrity assessment procedures.

At the same time, as far as the authors know, there is no research analysing the use of FADs in the assessment of 3D printed (fused deposition modelling) polymers and polymer-matrix composites. In this sense, additive manufacturing (AM) is a growing technology that allows complex geometries to be generated using a relatively simple method. Among the different AM technologies, fused deposition modelling (FDM) is the most extensively used. It consists in the extrusion of heated feedstock plastic filaments through a nozzle tip. The extruded material is placed layer by layer to generate the final piece according to a previously defined digital model (e.g., [19]). So far, the resulting materials have been basically used in prototyping, with an industrial interest in using them in applications with structural purposes. However, the use of FDM polymeric and polymer-matrix materials in structural applications requires the development of specific structural integrity assessment criteria.

With all this, the present work provides an approach to the structural integrity analysis of FDM materials containing notches, covering the two resulting simultaneous issues: the use of FADs in non-sharp defects (i.e., notches), and the application of FADs to (non-metallic) FDM materials. Thus, section 2 provides a brief theoretical background about FADs, the TCD and their combination to evaluate notch-type defects, section 3 describes the materials being analyzed and the methods used in the analyses, section 4 gathers the results and the corresponding discussion, and section 5 presents the main conclusions.

## 2. Theoretical background.

### 2.1. Failure assessment Diagrams

Failure Assessment Diagrams (FADs) are the main engineering tool for the analysis of fracture-plastic collapse in structural components containing crack-like defects. They provide a joint analysis of fracture and plastic collapse through two normalized parameters,  $K_r$  and  $L_r$ :

$$K_r = \frac{K_I}{K_{mat}} \quad (1)$$

$$L_r = \frac{P}{P_L} \quad (2)$$

where  $K_I$  is the stress intensity factor and  $K_{mat}$  is the material fracture resistance in terms of stress intensity factor units.  $K_{mat}$  may be linear-elastic (e.g.,  $K_{IC}$  [20]) or elastic-plastic (e.g.,  $K_{Jc}$ , derived from a critical value of the J-integral [21]). Additionally, P is the applied load and  $P_L$  is the limit load ( $L_r$  can also be defined as the ratio of the reference stress to the material yield stress [3]). Consequently,  $K_r$  evaluates the (cracked) component against fracture, whereas  $L_r$  evaluates the (cracked) component against plastic collapse.

$K_r$  and  $L_r$  constitute the coordinates of the resulting assessment point, which have to be compared with the limiting conditions defined by the Failure Assessment Line (FAL). Thus, when the assessment point is located above the FAL, the component is considered to be under unsafe conditions, whereas if the assessment point is located within the area defined by the FAL and the coordinate axes, the component is considered to be under safe conditions. Finally, the failure condition is established when the assessment point lies exactly on the FAL [1–5]. The general equation followed by the FAL is:

$$K_r = f(L_r) \quad (3)$$

Assessment procedures [1–5] provide solutions for the  $f(L_r)$  functions, which are essentially plasticity corrections to the conventional fracture assessment that compares the applied stress intensity factor with the material fracture toughness ( $K_I = K_{mat}$  or  $K_r = 1$ ). Here, it should be noted that the use of the plasticity correction allows a linear-elastic parameter ( $K_I$ ) to be used, regardless of the plasticity level on the crack tip. The exact solution of  $f(L_r)$  is:

$$f(L_r) = \sqrt{\frac{J_e}{J}} \quad (4)$$

where J is the applied J-integral and  $J_e$  is the elastic component of J. This equation corresponds, for instance, to FITNET FFS Procedure Option 4

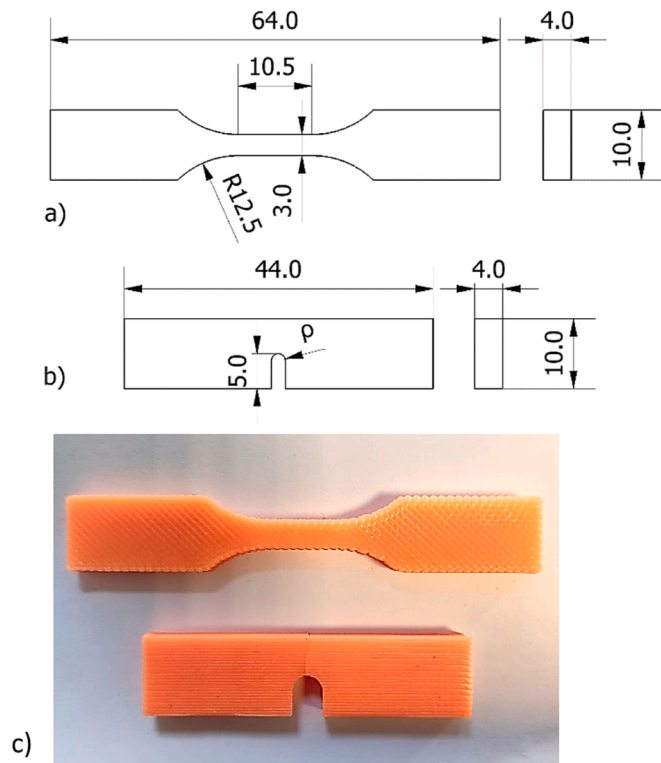


Fig. 1. Geometry of the ABS specimens. Dimensions in mm.: a) tensile specimens; b) fracture specimens ( $p$  ranging from 0 mm up to 2 mm. Span = 40 mm); c) images of a tensile specimen and a tested fracture notched specimen.

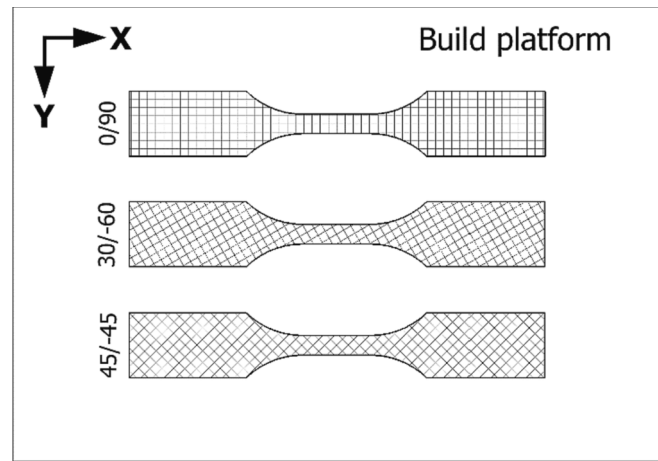


Fig. 2. Schematic of the different raster orientations.

[1,2] and BS 7910 Option 3 FAD [3]. Given the practical complexity of defining equation (4) in practical situations, these procedures also provide approximate solutions that are simply defined from the tensile properties of the material. These alternative FALS are usually provided hierarchically, defining different levels for which the more defined the material stress–strain curve, the more approximate are such solutions to equation (4). For example, both BS 7910 and FITNET FFS define Option 1, which only requires the yield (or proof) strength ( $\sigma_y$ ), the ultimate tensile strength ( $\sigma_u$ ) and the Youngs modulus (E). For those materials presenting continuous yielding (i.e., no yield plateau), Option 1 follows equations (5) to (10):

$$K_r = f(L_r) = (1 + 0.5 \cdot L_r^2)^{-1/2} \cdot \{0.3 + 0.7 \exp(-\mu L_r^6)\} \quad L_r \leq 1 \quad (5)$$

$$K_r = f(L_r) = f(1) \cdot L_r^{\frac{N-1}{N}} \quad 1 \leq L_r \leq L_{r, \max} \quad (6)$$

$$K_r = f(L_r) = 0 \quad L_r = L_{r, \max} \quad (7)$$

$$L_{r, \max} = \frac{\sigma_y + \sigma_u}{2 \cdot \sigma_y} \quad (8)$$

$$\mu = \min \left[ 0.001 \cdot \frac{E}{\sigma_y}; 0.6 \right] \quad (9)$$

$$N = 0.3 \cdot \left( 1 - \frac{\sigma_y}{\sigma_u} \right) \quad (10)$$

Equations (9) and (10), which define material parameters  $\mu$  and  $N$ , have been specifically calibrated and validated for metallic materials [22–25]. This original calibration is the major reason why assessment procedures such as BS7910 and FITNET FFS Procedure do not consider the fracture assessment of non-metallic materials.

In case of using the complete stress–strain curve of the material being analyzed, BS7910 [3] and FITNET FFS Procedure [1,2] provide analysis

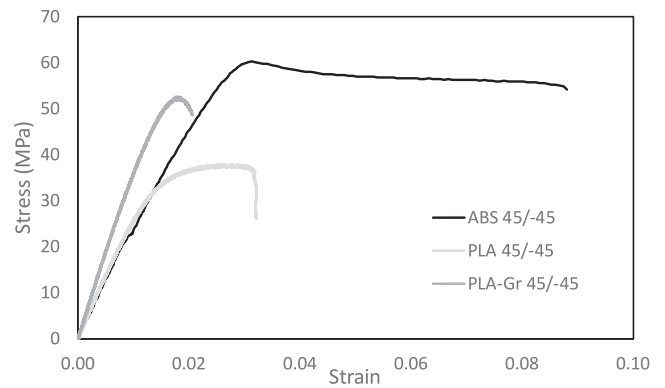


Fig. 3. Examples of stress–strain curves obtained in ABS, PLA and PLA-Gr materials. Raster orientation 45/-45 in all cases.

Table 1

Mechanical properties per material and raster orientation (average and standard deviation), and L values derived from the best fitting of experimental fracture results derived from ASTM D6068 and ASTM D5045.

Material	Raster orientation	E (MPa)	$\sigma_y$ (MPa)	$\sigma_u$ (MPa)	$e_{\max}$ (%)	L (mm)	
						ASTM D6068	ASTM D5045
ABS	0/90	2241 ± 169	51,8 ± 4,1	51,8 ± 4,1	2,9 ± 0,3	0.92	2.68
	30/-60	2329 ± 46	59,4 ± 1,1	59,4 ± 1,1	2,9 ± 0,2	0.45	2.84
	45/-45	2388 ± 182	60,9 ± 1,1	60,9 ± 1,1	3,1 ± 0,0	0.55	3.22
PLA	0/90	3769 ± 218	51,2 ± 0,9	52,0 ± 0,9	1,7 ± 0,2	0.53	0.57
	30/-60	3313 ± 212	38,0 ± 3,7	42,0 ± 3,0	1,9 ± 0,1	0.38	0.38
	45/-45	2751 ± 406	35,3 ± 4,6	41,1 ± 5,7	2,6 ± 0,2	0.20	0.24
PLA-Gr	0/90	4135 ± 277	50,5 ± 4,1	51,0 ± 4,4	1,4 ± 0,3	0.75	0.85
	30/-60	4065 ± 362	41,0 ± 2,7	44,3 ± 2,3	1,6 ± 0,2	0.81	2.28
	45/-45	3972 ± 260	47,5 ± 1,4	49,0 ± 2,8	1,5 ± 0,2	1.06	1.11

**Table A1**

Fracture toughness results on each individual test following ASTM D 6068 and ASTM D5045 standards, and experimental critical loads ( $P_{max}$ ). ABS material.

	Raster orientat	$\rho$ (mm)	Test	$P_{max}$ (N)	$P_{max}/P_Q$	$P_{max,avg}$ (N)	$K_{mat}^N$	$K_{mat,avg}^N$	$K_{mat}^N$	$K_{mat,avg}^N$
							(MPam <sup>1/2</sup> ) ASTM6068	(MPam <sup>1/2</sup> ) ASTM6068	(MPam <sup>1/2</sup> ) ASTM5045	(MPam <sup>1/2</sup> ) ASTM5045
ABS	0/90	0.00	1	84.92	1.04	82.12	3.43	3.54	2.23	2.05
		0.00	2	75.33	1.09		3.49		1.91	
		0.00	3	86.12	1.12		3.69		2.01	
		0.25	1	89.93	–	89.71	3.76	3.72	2.10	2.07
		0.25	2	89.48			3.68		2.03	
		0.50	1	98.19		95.91	4.16	4.04	2.07	2.09
		0.50	2	93.63			3.92		2.11	
		1.00	1	85.95		88.24	3.61	3.62	2.00	2.14
		1.00	2	90.52			3.62		2.29	
		2.00	1	101.33		102.15	4.54	4.51	2.20	2.24
	2.00	2	102.97			4.47		2.28		
	30/-60	0.00	1	69.83	1.24	85.67	3.78	3.98	1.59	1.99
		0.00	2	99.59	1.17		4.28		2.23	
		0.00	3	87.60	1.10		3.89		2.16	
		0.25	1	103.40	–	100.62	4.68	4.51	1.63	1.74
		0.25	2	97.83			4.33		1.85	
		0.50	1	100.45		100.80	4.46	4.51	2.28	2.24
		0.50	2	101.14			4.55		2.20	
		1.00	1	107.68		108.93	4.92	5.16	2.19	2.08
		1.00	2	110.18			5.39		1.96	
		2.00	1	111.93		111.77	5.41	5.62	2.22	2.15
	45/-45	0.00	1	70.50	1.15	86.11	3.82	4.12	1.94	2.03
		0.00	2	93.42	1.22		4.42		1.93	
		0.00	3	94.41	1.17		4.11		2.22	
		0.25	1	103.18	–	104.85	4.93	4.95	2.21	2.10
		0.25	2	106.52			4.97		1.99	
		0.50	1	108.21		105.74	4.89	4.73	2.16	2.12
		0.50	2	103.27			4.56		2.07	
		1.00	1	108.77		108.17	5.09	5.01	2.01	2.01
		1.00	2	107.56			4.92		2.02	
2.00		1	112.90		113.84	5.44	5.51	2.30	2.21	
2.00	2	114.77			5.57		2.12			

levels (options) 2 and 3, respectively, where  $f(L_r)$  follows equations (11) and (12):

$$f(L_r) = \left( \frac{E\epsilon_{ref}}{L_r\sigma_y} + \frac{L_r^3\sigma_y}{2E\epsilon_{ref}} \right)^{-1/2} \quad L_r \leq L_{r,max} \tag{11}$$

$$f(L_r) = 0 \quad L_r > L_{r,max} \tag{12}$$

where  $\epsilon_{ref}$  is the true strain at the true stress  $\sigma_{ref} = L_r\sigma_y$ .

In practice, Option 1 FAD is the most simple analysis option of BS 7910, yet providing accurate results. Therefore, it is the most commonly used by industry. Although structural integrity assessment procedures only cover the analysis of metallic materials when using this approach, there is theoretical and experimental evidence on its suitability for non-metallic materials [8,17,18].

2.2. The Theory of critical Distances

The Theory of Critical Distances (TCD) is actually a set of methodologies, all of them using a characteristic material length parameter, the critical distance (L), when performing fracture and fatigue assessments [6]. The origins of the TCD date back to the middle of the twentieth century, with the works of Neuber [26] and Peterson [27], but it has been in the last three decades when this theory has been comprehensively analyzed, establishing its applicability to different types of materials, processes and conditions. Recently, the authors have extended the use of the TCD to environmentally assisted cracking [28].

The expression for the critical distance in fracture analyses is:

$$L = \frac{1}{\pi} \left( \frac{K_{mat}}{\sigma_0} \right)^2 \tag{13}$$

where  $K_{mat}$  is the material fracture toughness in cracked conditions and  $\sigma_0$  is the material inherent strength, which is usually larger than the ultimate tensile strength ( $\sigma_u$ ) and requires calibration. L has analogous expressions in fatigue and environmentally assisted cracking analyses.

Among the different TCD methodologies, the Point Method (PM) and the Line Method (LM), both based on the stress-strain field on the notch tip, are particularly simple to apply. The PM states that fracture takes place when the stress equates the inherent strength ( $\sigma_0$ ) at a given distance (L/2) from the defect tip [6]:

$$\sigma\left(\frac{L}{2}\right) = \sigma_0 \tag{14}$$

Meanwhile, the LM states that fracture takes place when the average stress along a given distance from the defect tip (2L) equates  $\sigma_0$  [6]:

$$\frac{1}{2L} \int_0^{2L} \sigma(r)dr = \sigma_0 \tag{15}$$

Moreover, when combining these two methodologies with the stress distribution on the notch tip provided by Creager and Paris [29] (equation (16)), it is possible to obtain expressions (equations (17) and (18) for the PM and the LM, respectively) for the apparent fracture toughness ( $K_{mat}^N$ ) exhibited by materials containing U-shaped notches [6].

$$\sigma(r) = \frac{K_I}{\sqrt{\pi}} \frac{2(r+\rho)}{(2r+\rho)^{3/2}} \tag{16}$$

$$K_{mat}^N = K_{mat} \frac{\left(1 + \frac{\rho}{L}\right)^{3/2}}{\left(1 + \frac{2\rho}{L}\right)} \tag{17}$$

**Table A2**

Fracture toughness results on each individual test following ASTM D 6068 and ASTM D5045 standards, and experimental critical loads ( $P_{max}$ ). PLA material.

	Raster orientation	$\rho$ (mm)	Test	$P_{max}$ (N)	$P_{max}/P_Q$	$P_{max,avg}$ (N)	$K_{mat}^N$	$K_{mat,avg}^N$	$K_{mat}^N$	$K_{mat,avg}^N$
							(MPam <sup>1/2</sup> ) ASTM6068	(MPam <sup>1/2</sup> ) ASTM6068	(MPam <sup>1/2</sup> ) ASTM5045	(MPam <sup>1/2</sup> ) ASTM5045
PLA	0/90	0.00	1	177.4	1.13	188.15	5.59	5.61	3.24	3.46
		0.00	2	175.6	1.14		5.28		3.16	
		0.00	3	204.2	1.04		5.89		3.95	
		0.00	4	195.4	1.09		5.68		3.48	
		0.25	1	238.0	–	230.38	7.01	6.76	4.64	4.55
		0.25	2	217.9			6.29		4.39	
		0.25	3	235.2			6.99		4.61	
		0.25	4	–			–		–	
		0.50	1	256.9		249.56	7.09	7.06	5.08	4.76
		0.50	2	242.3			6.84		4.83	
		0.50	3	249.4			7.24		4.37	
		0.50	4	–			–		–	
		1.00	1	266.2		268.56	7.47	7.32	4.53	5.01
		1.00	2	287.6			8.27		4.73	
		1.00	3	262.2			6.87		5.19	
		1.00	4	258.2			6.68		5.58	
	2.00	1	215.6		205.94	7.40	7.25	4.01	3.91	
	2.00	2	200.7			6.91		4.04		
	2.00	3	211.4			8.10		3.79		
	2.00	4	196.1			6.59		3.80		
	30/-60	0.00	1	156.6	1.23	168.56	5.76	5.77	2.95	3.18
		0.00	2	184.2	1.06		5.54		3.71	
		0.00	3	162.8	1.18		5.61		3.12	
		0.00	4	170.6	1.23		6.15		2.92	
		0.25	1	204.4	–	231.36	6.01	6.48	3.88	4.43
		0.25	2	242.5			6.47		5.03	
		0.25	3	247.2			6.96		4.36	
		0.25	4	–			–		–	
		0.50	1	250.9		242.18	6.85	6.78	5.04	4.81
		0.50	2	240.7			7.09		4.46	
		0.50	3	234.7			6.35		4.77	
		0.50	4	242.5			6.81		4.95	
		1.00	1	281.9		26–2.89	9.16	8.17	4.80	4.84
		1.00	2	262.8			8.19		5.44	
		1.00	3	257.5			7.71		4.51	
		1.00	4	249.3			7.64		4.60	
	2.00	1	213.5		209.64	8.54	8.21	4.22	3.88	
	2.00	2	204.9			8.43		3.32		
	2.00	3	205.0			7.96		3.99		
	2.00	4	215.2			7.92		3.99		
	45/-45	0.00	1	148.6	1.10	147.29	5.12	4.91	2.89	2.82
		0.00	2	135.2	1.19		4.65		2.50	
		0.00	3	138.6	1.10		4.67		2.74	
		0.00	4	166.8	1.12		5.20		3.13	
		0.25	1	238.8	–	246.03	6.27	6.34	4.66	4.75
		0.25	2	235.1			6.40		4.78	
		0.25	3	266.6			6.43		5.23	
		0.25	4	243.6			6.26		4.33	
0.50		1	241.6		256.11	6.25	6.97	4.88	4.70	
0.50		2	267.7			7.66		4.40		
0.50		3	249.2			6.83		4.39		
0.50		4	265.9			7.13		5.13		
1.00		1	309.6		286.82	8.16	8.32	5.73	5.08	
1.00		2	289.4			8.57		5.19		
1.00		3	284.8			8.82		4.89		
1.00		4	263.5			7.73		4.51		
2.00	1	196.0		211.72	8.10	8.28	3.64	3.57		
2.00	2	219.4			9.24		3.20			
2.00	3	221.4			7.95		3.37			
2.00	4	210.1			7.81		4.08			

$$K_{mat}^N = K_{mat} \sqrt{1 + \frac{\rho}{4L}} \tag{18}$$

In equation (16),  $K_I$  is the mode I stress intensity factor,  $\rho$  is the notch radius and  $r$  is the distance from the notch tip to the point being assessed. In purely linear-elastic conditions, once  $K_{mat}^N$  is obtained, fracture analysis is performed by equating  $K_I$  to  $K_{mat}^N$ .

### 2.3. Assessment of notches combining FADs and the TCD

The TCD substitutes the real situation of a notched material whose fracture toughness is  $K_{mat}$ , by an equivalent situation of a cracked material (on which  $K_I$  may be easily defined in most practical cases) whose fracture resistance is  $K_{mat}^N$ . Thus, the notch correction may be introduced in the  $K_r$  parameter, combining the TCD with the FAD methodology [8]. The  $K_r$  parameter in notch analysis results:

**Table A3**

Fracture toughness results on each individual test following ASTM D 6068 and ASTM D5045 standards, and experimental critical loads ( $P_{max}$ ). Graphene reinforced PLA material.

	Raster orientation	$\rho$ (mm)	Test	$P_{max}$ (N)	$P_{max}/P_Q$	$P_{max,avg}$ (N)	$K_{mat}^N$	$K_{mat,avg}^N$	$K_{mat}^N$	$K_{mat,avg}^N$	
							(MPam <sup>1/2</sup> ) ASTM6068	(MPam <sup>1/2</sup> ) ASTM6068	(MPam <sup>1/2</sup> ) ASTM5045	(MPam <sup>1/2</sup> ) ASTM5045	
PLA-Gr	0/90	0.00	1	168.0	1.05	151.25	5.55	5.61	3.53	3.15	
		0.00	2	144.2	1.14		5.45		2.68		
		0.00	3	147.1	1.17		5.95		3.07		
		0.00	4	145.7	1.01		5.50		3.30		
		0.25	1	188.9	-	192.80	5.82	6.11	3.57	3.75	
		0.25	2	194.3			6.25		3.91		
		0.25	3	197.9			6.22		3.95		
		0.25	4	190.1			6.15		3.55		
		0.50	1	196.3		201.00	6.24	6.61	4.17	3.96	
		0.50	2	193.1			6.71		3.85		
		0.50	3	205.5			6.84		3.91		
		0.50	4	209.1			6.64		3.90		
		1.00	1	218.0		217.03	7.48	7.19	4.05	4.20	
		1.00	2	215.1			7.20		4.26		
		1.00	3	216.5			7.18		3.84		
		1.00	4	218.5			6.88		4.64		
		2.00	1	169.2		173.00	6.64	6.65	3.51	3.38	
		2.00	2	167.6			6.95		3.06		
		2.00	3	184.0			7.26		3.32		
		2.00	4	171.2			5.73		3.62		
		30/-60	0.00	1	195.3	1.10	189.03	7.06	6.92	3.71	3.71
				2	207.3	1.24		7.16		3.49	
				3	179.2	1.07		6.90		3.96	
				4	174.3	1.16		6.55		3.69	
	0.25			1	220.2	-	236.33	6.94	7.40	3.98	4.46
	0.25			2	245.7			7.82		4.15	
	0.25			3	245.4			7.59		5.10	
	0.25			4	234.0			7.24		4.59	
	0.50			1	262.2		243.50	8.07	7.56	5.39	4.67
	0.50			2	226.2			6.81		4.34	
	0.50			3	245.6			7.64		3.91	
	0.50			4	240.0			7.71		5.02	
	1.00		1	284.2		269.85	8.47	8.76	4.95	4.63	
	1.00		2	276.1			10.16		4.79		
	1.00		3	277.3			8.70		4.79		
	1.00		4	241.8			7.72		4.01		
	2.00		1	230.5		208.87	9.86	8.26	3.38	3.39	
	2.00		2	195.7			7.71		3.35		
	2.00		3	211.5			8.01		3.40		
	2.00		4	197.8			7.47		3.44		
	45/-45		0.00	1	163.3	1.28	189.18	7.58	7.20	3.67	3.73
				2	168.6	1.16		7.38		3.48	
				3	161.0	1.11		7.03		3.96	
				4	170.8	1.11		6.79		3.81	
		0.25		1	254.0	-	251.93	7.95	7.66	5.03	4.88
		0.25		2	253.7			7.48		4.85	
		0.25		3	252.6			7.62		4.69	
		0.25		4	247.4			7.58		4.97	
0.50		1		265.9		267.50	8.01	8.29	5.09	5.06	
0.50		2		263.0			7.87		5.11		
0.50		3		274.1			8.65		5.18		
0.50		4		267.0			8.62		4.87		
1.00		1	265.0		272.65	8.73	8.55	4.48	4.44		
1.00		2	263.8			8.15		4.34			
1.00		3	280.9			8.65		4.48			
1.00		4	280.9			8.65		4.48			
2.00		1	212.1		216.65	8.12	8.19	3.82	3.80		
2.00		2	222.6			7.99		4.11			
2.00		3	218.2			8.85		3.69			
2.00		4	213.7			7.78		3.57			

$$K_r = \frac{K_I}{K_{mat}^N} \tag{19}$$

Concerning the  $L_r$  parameter, plastic collapse occurs through the yielding of the remnant section, so that in a perfectly plastic material the limit load can be defined by the material yield stress and the defect in-plane dimensions, with a not very significant influence of the radius existing on the defect tip [8]. Therefore, the definition of  $L_r$  is the same

as that used for cracks (equation (2)), with available solutions in the literature for most of the practical situations.

Now, if the LM is applied equation (19) becomes:

$$K_r = \frac{K_I}{K_{mat}^N} = \frac{K_I}{K_{mat} \sqrt{1 + \frac{P}{4L}}} \tag{20}$$

Finally, regarding the FAL solutions to be used in the analysis of notches, [30] demonstrates the weak dependence of the  $f(L_r)$  on the

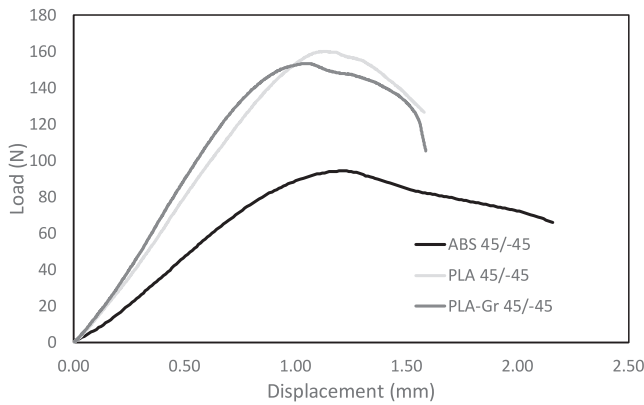


Fig. 4. Examples of load–displacement curves obtained in ABS, PLA and PLA-Gr materials (cracked conditions). Raster orientation 45/-45 in all cases.

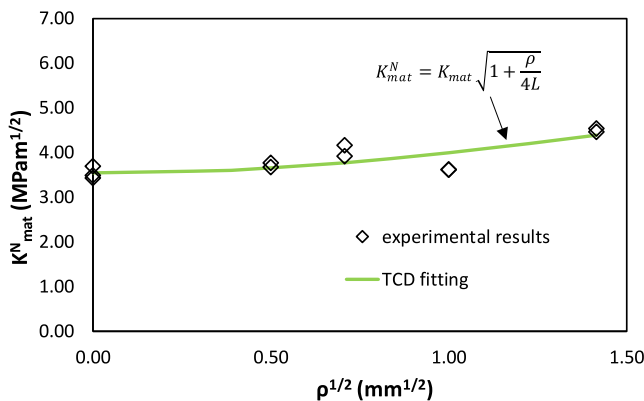


Fig. 5. Fitting of equation (18) to the experimental results of fracture resistance. ABS material, 0/90 raster orientation, ASTM D6068 fracture results.  $L = 0.92$  mm.

notch radius. In other words, when analyzing notches, it is possible to use the FALs proposed in structural integrity assessment procedures for the analysis of crack-like defects.

With all this, it may be concluded that the assessment of notches through Failure Assessment Diagrams only requires providing a correction of the material fracture resistance in the definition of the  $K_r$  parameter, using the apparent fracture toughness provided by (for example) the TCD instead of the material fracture toughness.

The combination of the FAD methodology and the TCD corrections for the structural integrity assessment of notches has been validated widely by the authors in fracture mechanics notched specimens (compact tension- CT and single edge notched bending- SENB) (e.g., [8,18]) and demonstrators [31].

### 3. Materials and methods

#### 3.1. Materials

This paper analyzes three different AM materials: ABS, PLA and graphene reinforced PLA. The printing parameters and experimental programs, among other details, are explained below.

##### 3.1.1. Abs

The experimental program was composed of 33 fracture tests (SENB specimens) and 9 tensile tests (see Fig. 1). The samples were fabricated by FDM, with the following printing parameters: layer height 0.3 mm, line width 0.4 mm, infill degree 100 %, printing temperature 230 °C, bed temperature 95 °C, and printing rate 40 mm/s. Three different raster

orientations were covered: 0/90, 30/-60 and 45/-45, as shown in the schematic gathered in Fig. 2. The resulting material had an area of internal voids up to 5%.

The notches of the SENB fracture specimens were machined, apart from those whose radius was 0 mm (crack-like defects), which were produced by sawing a razor blade. Fracture specimens covered five different notch radii: 0 mm, 0,25 mm, 0,50 mm, 1 mm and 2 mm. Two fracture tests were performed per combination of notch radius and raster orientation, except for the case of cracked specimens, for which three tests were tested per raster orientation.

Additional details may be found in [32].

##### 3.1.2. PLA

60 fracture tests and 9 tensile tests were printed with the PLA material, considering the same three different raster orientations (0/90, 30/-60 and 45/-45) mentioned above and, for the fracture specimens, covering the same five different notch radii (0 mm, 0.25 mm, 0.5 mm, 1 mm and 2 mm). The geometry of the specimens is the same as that shown in Fig. 1 for ABS specimens. Three tensile tests were performed per raster orientation and four fracture tests were done per combination of notch radius ( $\rho$ ) and raster orientation.

The notches were machined, excluding the 0 mm radius defects, which were generated by sawing a razor blade. All samples were manufactured by FDM with the following printing parameters: layer height 0.3 mm, nozzle diameter 0.4 mm, infill level 100%, printing temperature 200 °C, bed temperature 75 °C, and printing rate 30 mm/s. The percentage of internal voids was generally lower than 1%.

Additional details are gathered in [33].

##### 3.1.3. Graphene-reinforced PLA

The experimental programme on graphene-reinforced PLA (PLA-GR) follows an identical approach as that explained above for PLA material. The only difference is the material used in the printing process, which in this case is the same PLA with a graphene content of 1 wt% (see [33] for further details). Again, the percentage of internal voids was generally lower than 1%.

### 3.2. Methods

Tensile tests were performed at room temperature following ASTM D638 [34], whereas fracture tests were performed at room temperature on three-point bending specimens (SENB) and were subsequently analyzed through ASTM D5045 [35] and ASTM D6068 [36] standards. The reason for this double fracture analysis is that the curves obtained in the fracture tests of the SENB specimens containing cracks (those used in the fracture toughness characterization) provided  $P_{max}/P_Q$  [35] values close to 1.1 (validity limit in [35]), but often above this value, suggesting that linear-elastic fracture mechanics conditions were not always met. Thus, the fracture tests were also analyzed by applying [36], calculating the J-integral at final fracture (and subsequently converting J into  $K_J$ ) on the assumption that there were no previous stable crack propagations (this was confirmed through the observation of fracture surfaces [32,33]). In other words, given that, to the knowledge of the authors and for the materials being analyzed, there is no standard addressing the determination of an elastic-plastic value of the material toughness with negligible or limited tearing, we applied the J-R calculation procedure considering that there was no significant tearing before fracture.

For both tensile and fracture tests, the nominal dimensions of the specimens were considered in the analyses (i.e., the presence of internal voids was not considered). Thus, subsequent structural integrity assessments will also consider nominal dimensions.

Once the fracture tests on both cracked and notched specimens were completed, the value of L was experimentally fitted for the three materials and three raster orientations analyzed in this paper, with the analyses being described in [32] and [33].

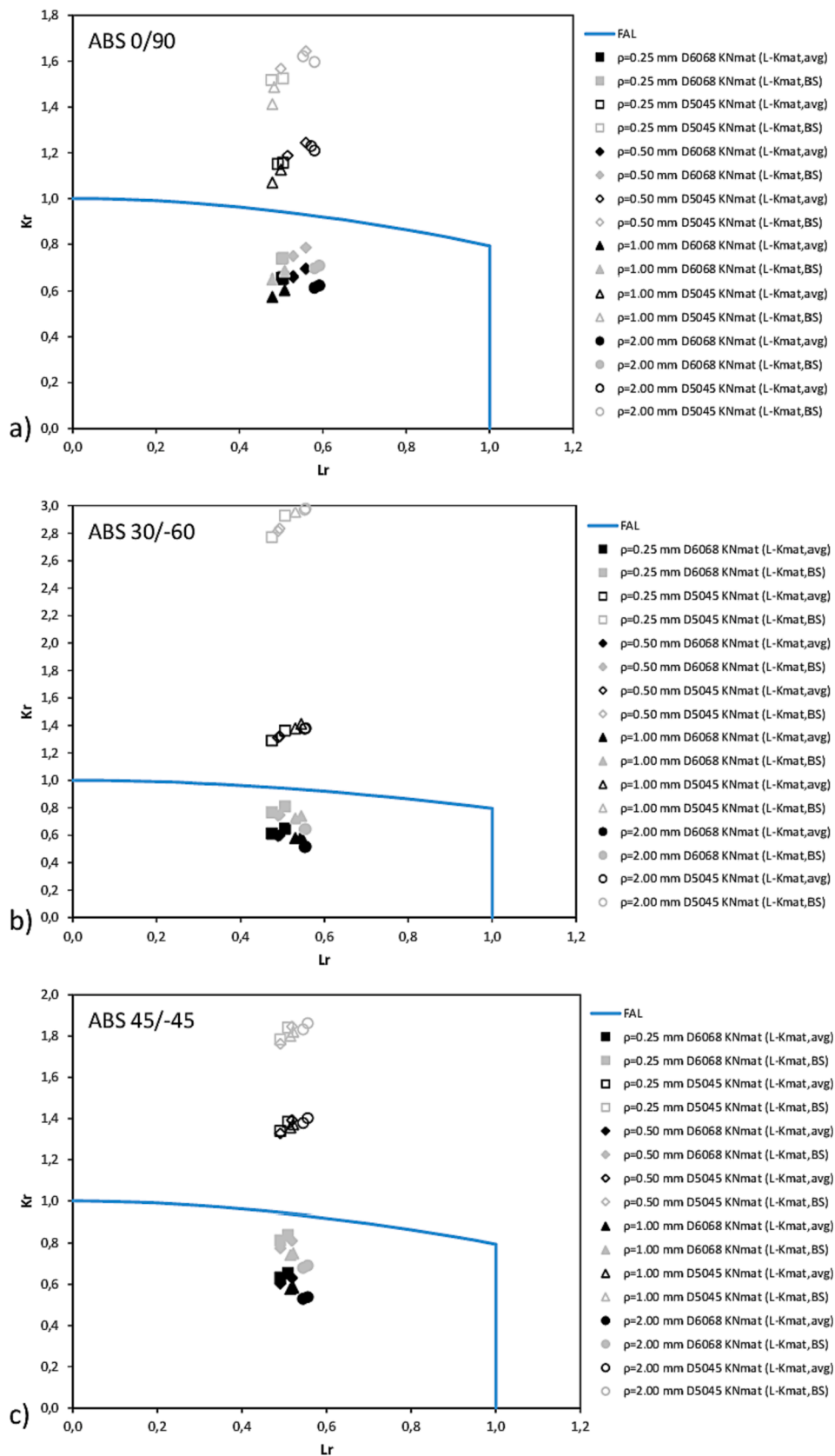


Fig. 6. FAD analysis of U-notched ABS specimens at failure. a) raster orientation 0/90; b) raster orientation 30/-60; raster orientation 45/-45.

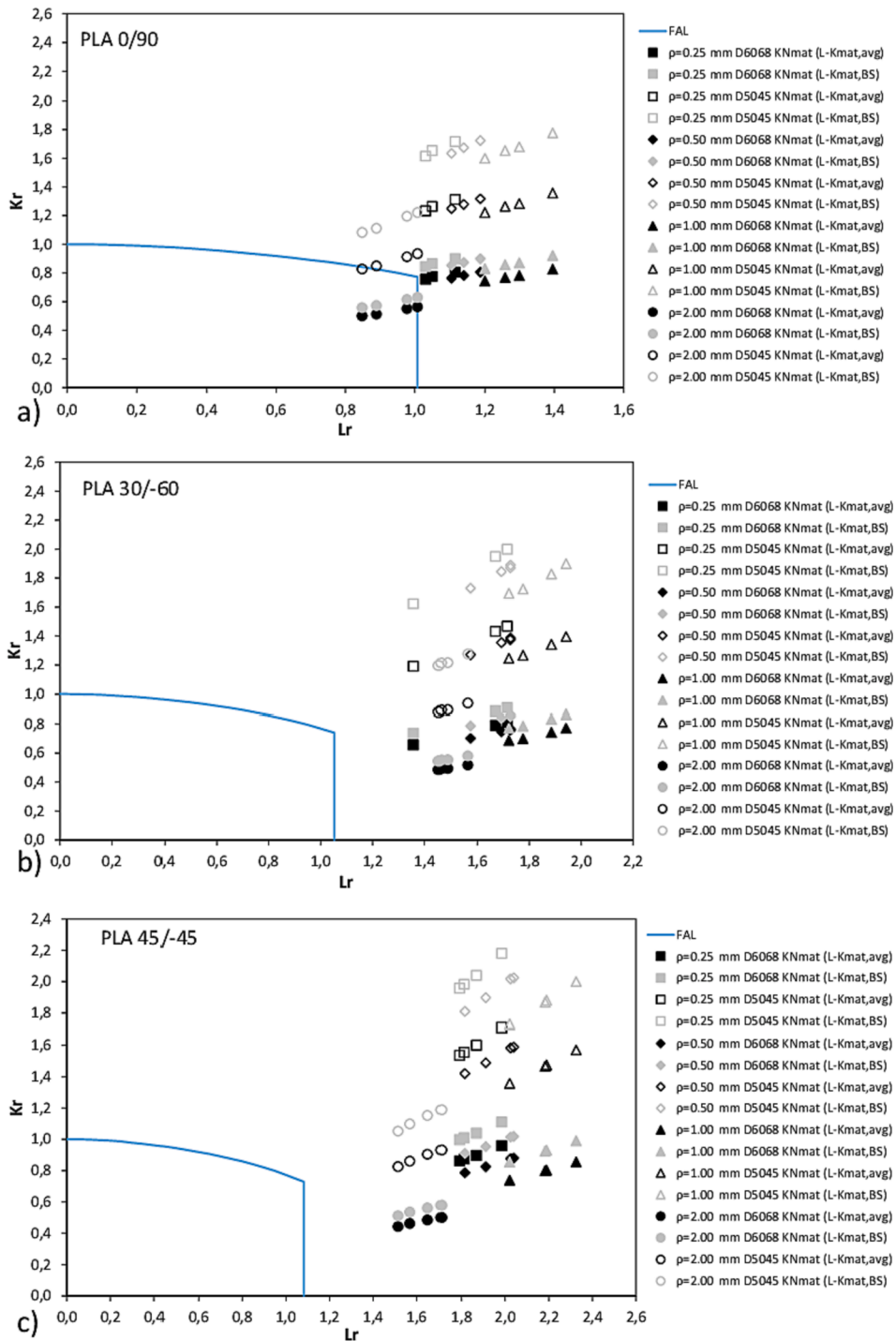


Fig. 7. FAD analysis of U-notched PLA specimens at failure. a) raster orientation 0/90; b) raster orientation 30/-60; raster orientation 45/-45.

Finally, the procedure described in Section 2.3 was applied to the notched specimens with the aim of providing a FAD assessment for each combination of material, raster orientation and notch radius. BS7910 Option 1 FAL was used in all cases,  $K_I$  solutions were taken from ASTM D5045 [35], whereas  $P_L$  solutions were taken from [37]. Here it should be noted that the notched fracture specimens were in an intermediate situation between plane stress and plane strain conditions, so the  $P_L$  used in the assessment was derived from the interpolation between the plane stress and plane strain solutions of  $P_L$  provided in [37]. Interpolation limits were given by equations (21) and (22) for plane strain and plane stress conditions, respectively [6]:

$$K_{mat}^N \leq \sigma_y \sqrt{\frac{B}{2.5}} \tag{21}$$

$$K_{mat}^N > \sigma_y \sqrt{\pi B} \tag{22}$$

#### 4. Results

Table 1 gathers the tensile properties of the different combinations of material and raster orientation, which are used in the FAD analysis [32,33].  $E$  is the Young's modulus,  $\sigma_y$  is the yield stress and  $\sigma_u$  is the tensile strength (or ultimate tensile strength). Fig. 3 shows some

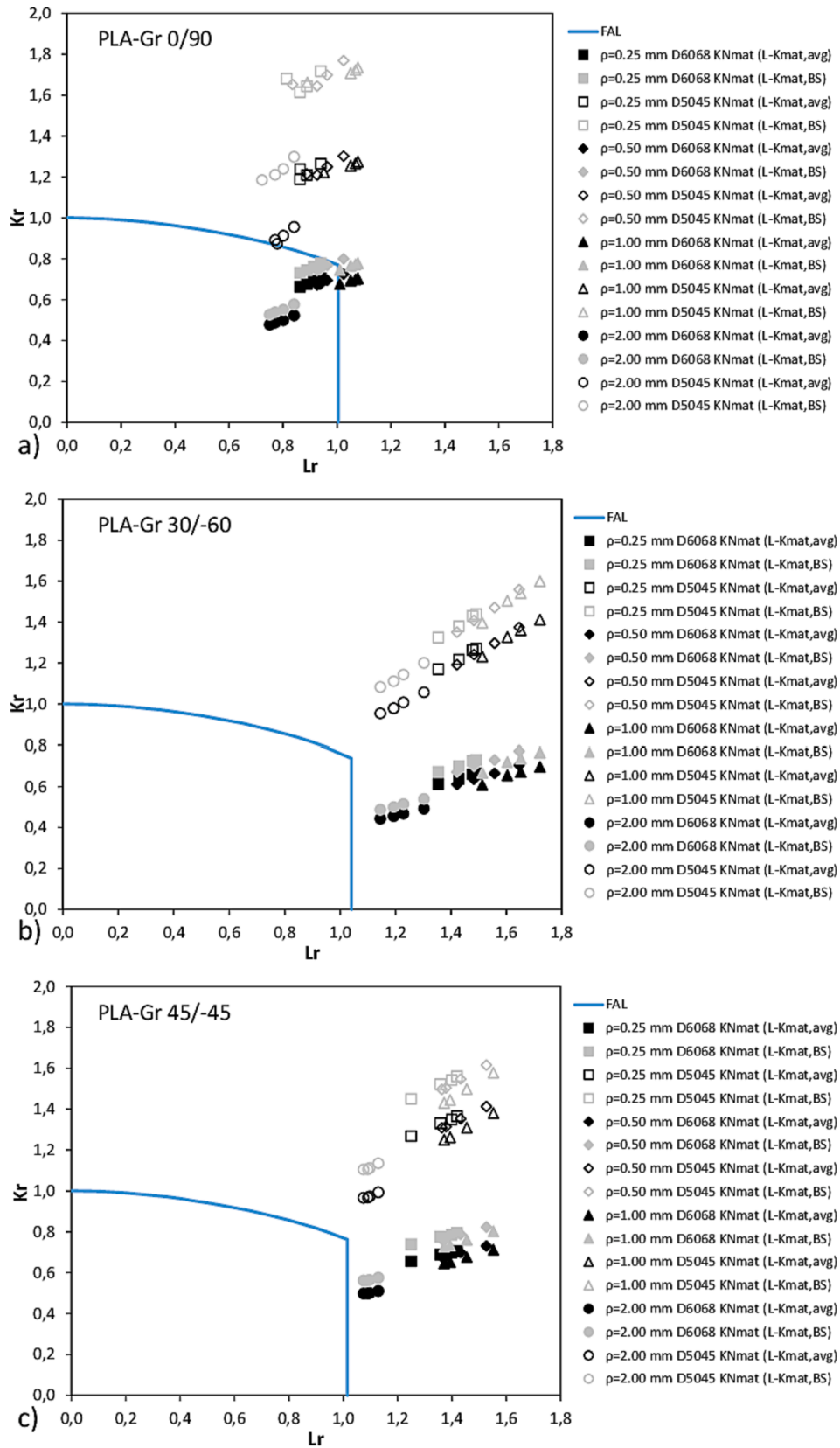


Fig. 8. FAD analysis of U-notched graphene reinforced PLA specimens at failure. a) raster orientation 0/90; b) raster orientation 30/-60; raster orientation 45/-45.

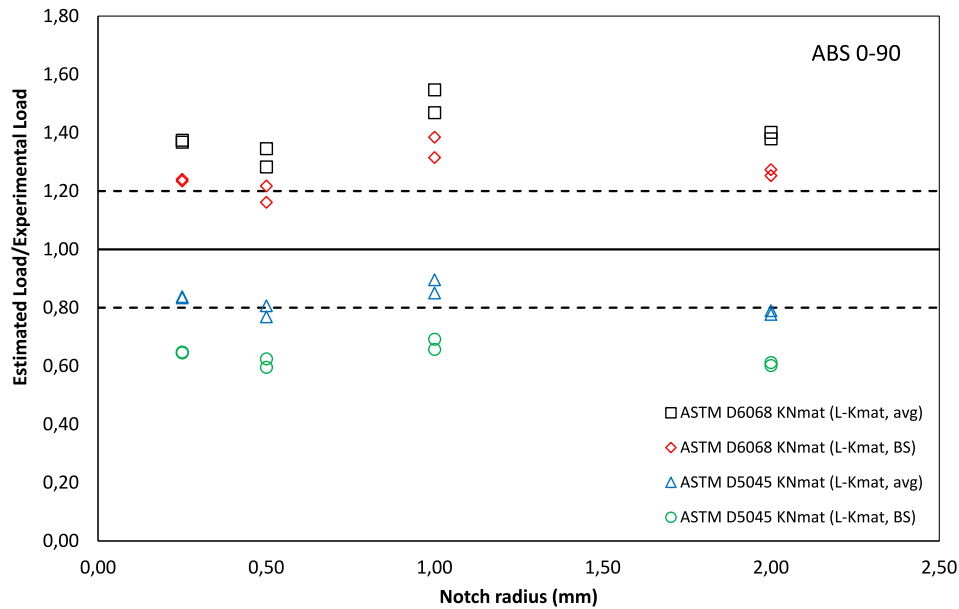


Fig. 9. Comparison between estimated (critical) loads and experimental critical loads for ABS notched material and raster orientation 0/90.

examples of stress–strain curves. The ABS materials present stress–strain curves with a maximum stress at yield, followed by softening. Thus, the tensile strength is the so called strength at yield [34] and coincides with the material yield stress. PLA and PLA-Gr materials have both increasing stress–strain curves till failure, with the yield stress defined by the 0.2% offset strength, and the tensile strength defined by the maximum stress level of the curves.

Tables A1 to A3 in Appendix A gather the results of the fracture tests, with the individual values of maximum load and the resulting fracture toughness following the two different standards used in the analyses (ASTM D5045 and ASTM D6068). Average values are also included. Fig. 4 shows examples of the obtained load–displacement curves.

It can be observed in Appendix A how the two standards provide noticeably different results, with ASTM D6068 leading to fracture toughness values that may be more than double those obtained through linear-elastic formulations (i.e., ASTM D5045). Moreover, there is a clear notch effect, with (generally) higher fracture loads and fracture toughness values when the notch radius increases. However, surprisingly, in PLA and PLA-Gr the fracture loads and the linear-elastic fracture toughness values are lower for a notch radius of 2.0 mm than for a notch radius of 1.0 mm. The observed notch effect is, in any case, more moderate than that observed in other materials, such as PMMA, Al alloys or structural steels [7].

For each material, the corresponding critical distance ( $L$ ) was calculated. With this aim, the fracture resistance values obtained for the different notch radii were graphically represented for each combination of material and raster orientation. Then,  $L$  was obtained by fitting equation (18) to the experimental results and by using the least squares method.  $K_{mat}$  in equation (18) was fixed at the average value of the corresponding fracture toughness results obtained in cracked specimens ( $\rho = 0$  mm). Given that two standards were applied to the experimental fracture results, two values of  $L$  were obtained per material and raster orientation. Fig. 5 shows an example, while Table 1 gathers the different  $L$  values. Here, it is worth mentioning that the fitting process could have been performed by using equation (17) (Point Method), instead of equation (18) (Line Method), providing very similar results. For the sake of simplicity, only the results obtained through equation (18) are included in this work.

Once the tensile properties, the fracture toughness ( $K_{mat}$ ) and  $L$  are known for each combination of material and raster orientation, the FAD approach described above (with equation (20) defining  $K_r$ ) can be easily

applied. Two values of  $K_{mat}$  will be used in the calculations: the average values ( $K_{mat,avg}$ ), which are gathered in Tables A1 to A3 when looking at the results obtained in cracked specimens ( $\rho = 0$  mm), and a conservative statistical value provided by BS7910,  $K_{mat,BS}$  (see section 7.1.7 in [3]). The average value tends to better capture the physics of the fracture processes being analyzed, whereas the statistical value is a conservative estimation used to derive safe predictions when applying structural integrity assessment procedures, and it is defined by equation (23):

$$K_{mat,BS} = K_{mat,avg} - k \hat{A} \cdot Sdv \quad (23)$$

$Sdv$  being the standard deviation and  $k$  being a coefficient defining the percentile of the distribution for which  $K_{mat,BS}$  is required with a given confidence. Typically, and here, the 20th lower percentile is used, with the corresponding  $k_{0,90}$  coefficients depending on the number of fracture tests performed and being provided by BS7910. In this particular work,  $k_{0,90}$  is 3.039 for ABS material (three fracture tests performed per raster orientation) and 2.295 for PLA and PLA-Gr materials (four fracture tests per raster orientation).

Figs. 6 to 8 show the FAD assessment of the different notched specimens at fracture load. The resulting assessment points should theoretically be located on the FAL, but the actual location of the points strongly depends on the criteria used to define  $K_{mat}$  (ASTM D5045 vs ASTM D6068, and average values vs. BS7910 statistical values). Here, it should be noted that when using one of the standards, the  $L$  value used in the notch correction included in  $K_r$  (equation (20)) is the one obtained through the fitting of fracture resistance results obtained when using that same standard.

It can be observed how the assessment points are generally located further away from the FAL as the notch radius increases. This is particularly clear in PLA, whereas in the case of ABS it is not so evident due to its lower notch effect (and larger  $L$ ).

The results show that using ASTM D6068 fracture toughness results (solid symbols) generates unsafe predictions on many occasions (e.g., ABS in all raster orientations, PLA and PLA-Gr in raster orientation 0/90), with the assessment points at fracture being located in the safe area of the FAD. This undesirable situation occurs regardless of the value of fracture toughness being used (average vs. statistical). The assessments where ASTM D6068 does not provide unsafe predictions (i.e., assessment points above the FAL) are those on which the  $L_r$  at failure is higher than  $L_{r,max}$  and, then, the collapse of the remnant section plays a key role

in the final failure.

On the contrary, the assessments provided when using ASTM D5045 fracture toughness results are usually safe. Just one assessment point, in PLA material and raster orientation 0/90, corresponds to an unsafe assessment on which the assessment point lies (slightly) below the FAL. In general, the combination of ASTM D5045 standard and average fracture toughness values provides safe assessment points which are often not too far from the FAL, thus providing an acceptable level of conservatism. However, the combination of ASTM D5045 standard with the statistical values of fracture toughness suggested by the BS7910 leads recurrently to overconservative results, with the assessment points being frequently located far from the FAL. Thus, combining ASTM D5045 fracture characterization processes and the resulting average values of fracture toughness has been the best combination in this research, providing the optimal equilibrium between safety and accuracy.

Fig. 9 presents an example of alternative (equivalent) assessment. Instead of representing the different specimens at fracture, the fracture load predicted by the FAD methodology may be calculated for each specimen (i.e., the load that places the assessment point on the FAL) by using the different criteria explained above, and then it can be compared to the experimental one. Again, when using ASTM D6068 fracture toughness results, the assessments are clearly unsafe, with predicted fracture loads that may be significantly higher than the experimental ones.

When applying ASTM D5045 fracture toughness results, the assessments are usually safe (except for the one case mentioned above). In the example of Fig. 9, the use of average values provides reasonable levels of conservatism (the ratio of predicted load to experimental load is around 0.8), whereas the use of statistical more conservative values of  $K_{mat}$  leads to an increased conservatism (in Fig. 9, the mentioned ratio ranges between 0.60 and 0.70). However, it still improves significantly the accuracy of the predictions when compared to those obtained through the assessment of notches as if they were cracks (i.e., without any notch correction), a practice that leads to higher levels of conservatism.

The results shown in this work, in which it has been observed that the validity range of ASTM D5045 (linear-elastic) was not met in many of the specimens, but also that ASTM D5045 and ASTM D6068 standards provide significantly different results even under linear elastic conditions criterion ( $P_{max}/P_Q < 1.1$ ), point to the need for future additional research into the reasons for such differences. The research should also determine why ASTM D6068 provides unsafe results in combination with the FAD approach, something that suggests that this standard is overestimating the corresponding values of the fracture toughness in this kind of materials. Here, it is worth mentioning that ASTM D6068 defines the experimental and analytical processes used to define the whole J-R curve of polymeric materials. However, the materials analyzed in this work do not (apparently) develop crack growth (although they may develop damage on the crack tip), so a single value of J (subsequently converted to  $K_I$ ) has been obtained at maximum load under the assumption that there was no stable crack propagation. This criterion has often led to unsafe fracture load predictions.

## 5. Conclusions

This paper provides a methodology for the assessment of U-notched additively manufactured polymers and polymer-matrix composites. The methodology is validated by using experimental results obtained in ABS, PLA and graphene-reinforced PLA, and consists in assessing the notched components by using Failure Assessment Diagrams on which the  $K_r$  parameter is modified with the aim of accounting for the notch effect: instead of using the fracture toughness ( $K_{mat}$ ) derived from fracture tests on cracked specimens when calculating the ratio  $K_r$  ( $K_I/K_{mat}$ ), the approach uses the predictions of apparent fracture toughness ( $K_{mat}^N$ ) provided by the Theory of Critical Distances. This requires a previous calibration of the material critical distance (L), but allows applying the

FAD methodology with this only modification.

It has been noted that, for the materials being analyzed, the fracture toughness results obtained from linear-elastic standard ASTM D5045 and elastic-plastic standard ASTM D6068 may have very significant differences. These differences are observed even in tests where linear-elastic conditions are strictly met, not only in those where ASTM D5045 is out of scope. Moreover, the particular application of ASTM D6068 performed in this work, which assumes that there has been no stable crack propagation before failure and calculates a single value of the J integral at fracture load, leads frequently to unsafe predictions of fracture loads, suggesting that this application of the standard is actually overestimating the fracture resistance of this type of materials. On the contrary, ASTM D5045 fracture results usually provide safe results, with acceptable levels of conservatism when the FAD analysis is performed using average values of  $K_{mat}$ . With all this, it is recommended to use ASTM D5045 (and not ASTM D6068) when characterizing FDM printed ABS, PLA and PLA-Gr materials, acknowledging the resulting conservatism of the results.

Further research is required to analyze the reasons justifying the differences between the fracture toughness results obtained when using the two standards.

## CRediT authorship contribution statement

**S. Cicero:** Conceptualization, Investigation, Methodology, Writing – original draft, Funding acquisition. **M. Sánchez:** Investigation, Data curation. **V. Martínez-Mata:** Investigation, Data curation. **S. Arrieta:** Investigation, Data curation. **B. Arroyo:** Investigation, Writing – review & editing.

## Declaration of Competing Interest

The authors declare that they have no known competing financial interests or personal relationships that could have appeared to influence the work reported in this paper.

## Acknowledgements

This publication is part of the project “Comportamiento en fractura de materiales compuestos nano-reforzados con defectos tipo entalla, PGC2018-095400-B-I00” funded by MCIN/AEI/10.13039/501100011033/FEDER “Una manera de hacer Europa”.

## Appendix A

### Fracture toughness results and experimental critical loads

(SEE Tables A1-A3).

## References

- [1] M. Kocak, S. Webster, J.J. Janosch, R.A. Ainsworth, R. Koers, FITNET fitness-for-service (FFS), procedure, Vol. 1, GKSS Hamburg, Germany, 2008.
- [2] F. Gutiérrez-Solana, S. Cicero, FITNET FFS Procedure: a unified european procedure for structural integrity assessment, Eng. Fail. Anal. 16 (2) (2009) 559–577, <https://doi.org/10.1016/j.engfailanal.2008.02.007>.
- [3] BS 7910:2019. Guide to methods for assessing the acceptability of flaws in metallic structures, British Standard Institution, London, UK, 2019.
- [4] R6, Rev.4. Assessment of the integrity of structures containing defects, EDF Energy, Gloucester, UK, 2014.
- [5] API RP 579-1 / ASME FFS-1. “API 579-1/ASME FFS-1, Third edition, The American Society of Mechanical Engineers, New York, USA, 2016.
- [6] D. Taylor, The theory of critical distances: a new perspective in fracture mechanics, Elsevier, UK, 2007.
- [7] S. Cicero, V. Madrazo, T. García, J. Cuervo, E. Ruiz, On the notch effect in load bearing capacity, apparent fracture toughness and fracture mechanisms of polymer PMMA, aluminium alloy Al7075-T651 and structural steels S275JR and S355J2, Eng. Fail. Anal. 29 (2013) 108–121.

- [8] S. Cicero, V. Madrazo, I.A. Carrascal, R. Cicero, Assessment of notched structural components using failure assessment diagrams and the theory of critical distances, *Eng. Fract. Mech.* 78 (2011) 2809–2825.
- [9] L.S. Niu, C. Chehimi, G. Pluvinage, Stress field near a large blunted V notch and application of the concept of notch stress intensity factor to the fracture of very brittle materials, *Eng. Fract. Mech.* 49 (1994) 325–335.
- [10] G. Pluvinage, Fatigue and fracture emanating from notch; the use of the notch stress intensity factor, *Nucl. Eng. Des.* 185 (1998) 173–184.
- [11] A. Hilleborg, M. Modeer, P.E. Petersson, Analysis of crack formation and crack growth in concrete by means of fracture mechanics and finite elements, *Cem. Concr. Res.* 6 (1976) 777–782.
- [12] F.J. Gomez, M. Elices, A. Valiente, Cracking in PMMA containing U-shaped notches, *Fat. Frac. Eng. Mat. Struct.* 23 (9) (2000) 795–803.
- [13] W. Weibull, The phenomenon of rupture in solids, *Proc. R. Swed. Inst. Eng. Res.* 153 (1939) 1–55.
- [14] F.M. Beremin, A. Pineau, F. Mudry, J.-C. Devaux, Y. D'Escatha, P. Ledermann, A local criterion for cleavage fracture of a nuclear pressure vessel steel, *Metall. Trans. A* 14 (11) (1983) 2277–2287.
- [15] G.C. Sih, Strain-energy-density factor applied to mixed mode crack problems, *Int. J. Fract.* 10 (3) (1974) 305–321.
- [16] F. Berto, P. Lazzarin, Recent developments in brittle and quasi-brittle failure assessment of engineering materials by means of local approaches, *Mater. Sci. Eng. R* 75 (2014) 1–48.
- [17] J.-J. Han, H.-W. Ryu, Y.-J. Kim, J.-S. Kim, Y.-J. Oh, H.-B. Park, Failure assessment diagram analysis of high density polyethylene pipes, *J. Mech. Sci.* 28 (12) (2014) 4929–4938, <https://doi.org/10.1007/s12206-014-1113-3>.
- [18] F.T. Ibañez-Gutiérrez, S. Cicero, Fracture assessment of notched short glass fibre reinforced polyamide 6: an approach from failure assessment diagrams and the theory of critical distances, *Compos. B Eng.* 111 (2017) 124–133, <https://doi.org/10.1016/j.compositesb.2016.11.053>.
- [19] T.D. Ngo, A. Kashani, G. Imbalzano, K.T.Q. Nguyen, D. Hui, Additive manufacturing (3D printing): a review of materials, methods, applications and challenges, *Composites Part B: Engineering* 143 (2018) 172–196, <https://doi.org/10.1016/j.compositesb.2018.02.012>.
- [20] ASTM International, E399–20a, Standard Test Method for Linear-Elastic Plane-Strain Fracture Toughness of Metallic Materials, Philadelphia, USA, 2020.
- [21] ASTM International, E1820–20, Standard Test Method for Measurement of Fracture Toughness, Philadelphia, USA, 2020.
- [22] J. Ruiz-Ocejo, F. Gutiérrez-Solana, M.A. González-Posada, Report/SINTAP/UC/06: structural integrity assessment procedures for European industry (SINTAP), University of Cantabria, Santander, Spain, 1998.
- [23] R.A. Ainsworth, F. Gutierrez-Solana, J.R. Ocejo, Analysis levels within the SINTAP defect assessment procedures, *Eng. Fract. Mech.* 67 (6) (2000) 515–527, [https://doi.org/10.1016/S0013-7944\(00\)00071-0](https://doi.org/10.1016/S0013-7944(00)00071-0).
- [24] J. Ruiz-Ocejo, F. Gutiérrez-Solana, M.A. González-Posada, Report/SINTAP/UC/08: structural integrity assessment procedures for European industry (SINTAP), University of Cantabria, Santander, Spain, 1998.
- [25] A.C. Bannister, J. Ruiz Ocejo, F. Gutierrez-Solana, Implications of the yield stress/tensile stress ratio to the SINTAP failure assessment diagrams for homogeneous materials, *Eng. Fract. Mech.* 67 (6) (2000) 547–562, [https://doi.org/10.1016/S0013-7944\(00\)00073-4](https://doi.org/10.1016/S0013-7944(00)00073-4).
- [26] H. Neuber, Theory of notch stresses: principles for exact calculation of strength with reference to structural form and material, Springer Verlag, Berlin, 1958.
- [27] R.E. Peterson, Notch sensitivity, in: G. Sines, J.L. Waisman (Eds.), Metal fatigue, McGraw Hill, New York, 1959, pp. 293–306.
- [28] P. González, S. Cicero, B. Arroyo, J.A. Álvarez, A theory of critical distances based methodology for the analysis of environmentally assisted cracking in steels, *Eng. Fract. Mech.* 214 (2019) 134–148.
- [29] M. Creager, P.C. Paris, Elastic field equations for blunt cracks with reference to stress corrosion cracking, *Int. J. Fract. Mech.* 3 (4) (1967) 247–252.
- [30] A.J. Horn, A.H. Sherry, An engineering assessment methodology for non-sharp defects in steel structures - Part I: procedure development, *Int. J. Press. Vessel. Pip.* 89 (2012) 137–150.
- [31] S. Cicero, M. Sanchez, B. Arroyo, J.D. Fuentes, J.A. Alvarez, Estimation of the load-bearing capacity of tubular cantilever beams containing through-thickness circumferential U-notches, *Eng. Struct.* 229 (2021), 111598.
- [32] S. Cicero, V. Martínez-Mata, A. Alonso-Estebanez, L. Castanon-Jano, B. Arroyo, Analysis of Notch Effect in 3D-Printed ABS Fracture Specimens Containing U-Notches, *Materials* 13 (2020) 4716, <https://doi.org/10.3390/ma13214716>.
- [33] S. Cicero, V. Martínez-Mata, L. Castanon-Jano, A. Alonso-Estebanez, B. Arroyo, Analysis of notch effect in the fracture behaviour of additively manufactured PLA and graphene reinforced PLA, *Theor. Appl. Fract. Mech.* 114 (2021), 103032.
- [34] ASTM, D638–14, Standard test method for tensile properties of plastics, ASTM International, West Conshohocken, PA, 2014.
- [35] ASTM D5045-14, Standard Test Methods for Plane-Strain Fracture Toughness and Strain Energy Release Rate of Plastic Materials, ASTM International, West Conshohocken, PA, 2014.
- [36] ASTM D6068-10(2018), Standard Test Method for Determining J-R Curves of Plastic Materials, ASTM International, West Conshohocken, PA, 2018.
- [37] T.L. Anderson, Fracture mechanics: fundamentals and applications, 4th ed., CRC Press - Taylor and Francis Group, Boca Raton, USA, 2005.